metals

MDPI

Article

Effect of Carburizing Composite Laser-Shock Processing on Properties and Microstructure of 20CrNiMo Steel

Xiuyu Chen *, Jie Sun, Kelin Li, Yuru Lin, Zhilong Xu *, Bicheng Guo, Junying Chen and Qingshan Jiang

College of Marine Equipment and Mechanical Engineering, Jimei University, Xiamen 361000, China; sunjie5535@163.com (J.S.); lkljmdx@163.com (K.L.); linyru_11@163.com (Y.L.); guobicheng@jmu.edu.cn (B.G.); chenjunying@jmu.edu.cn (J.C.); qs-bctf@163.com (Q.J.)

* Correspondence: jdcxy@126.com (X.C.); zhilong.xu@163.com (Z.X.)

Abstract: In the service process of gears, premature fatigue failure or fracture of gears is often caused by poor surface performance. 20CrNiMo steel is a commonly used material for gears. Laser-shock peening (LSP), carburizing treatment (CT), and hybrid modification of carburizing treatment and laser-shock peening (LSP + CT) were carried out to improve the performance of 20CrNiMo steel. The hardness, residual stress, microstructure, subgrain size, and toughness of the samples were analyzed following various modification methods. It was observed that the properties of the composite-modified gradient structure materials achieved through carburizing and laser-shock peening were superior to those modified using single methods. After the composite treatment of carburizing and laser shocking, the samples exhibited the most significant increase in hardness, up to 916HV0.1, with a surface layer experiencing residual compressive stress as low as −635 MPa. Simultaneously, a gradient microstructure was formed on the surface layer, with 80% of the crystallites being in the nanoscale range. Furthermore, the toughness was notably enhanced. Experimental results confirm the improvement in the properties of 20CrNiMo samples, resulting in the creation of a functionally graded material through the composite treatment of carburizing and laser shocking.

Keywords: carburizing; laser shocking; hybrid modification; functional gradient

check for updates

Citation: Chen, X.; Sun, J.; Li, K.; Lin, Y.; Xu, Z.; Guo, B.; Chen, J.; Jiang, Q. Effect of Carburizing Composite Laser-Shock Processing on Properties and Microstructure of 20CrNiMo Steel. *Metals* **2024**, *14*, 10. https://doi.org/10.3390/met14010010

Academic Editor: Angelo Fernando Padilha

Received: 11 October 2023
Revised: 3 December 2023
Accepted: 5 December 2023
Published: 21 December 2023

Copyright: © 2023 by the authors. Licensee MDPI, Basel, Switzerland. This article is an open access article distributed under the terms and conditions of the Creative Commons Attribution (CC BY) license (https://creativecommons.org/licenses/by/4.0/).

1. Introduction

20CrNiMo steel, as like AISI 8620 steel, has high strength and toughness, good hardenability, good fatigue resistance, and excellent comprehensive mechanical properties [1]. In service, the root gear bears sudden impact and periodic bending stress; meanwhile, the gear surface takes contact stress. Due to insufficient surface performance, 20CrNiMo gears are prone to premature bending fatigue failure, contact fatigue failure, or brittle fracture of gears [2]. The failure of the gear causes the collapse of the entire transmission system, resulting in safety accidents and economic losses [3]. Surface chemical heat treatment and surface strain-strengthening treatment are widely used to improve the surface properties of metal components [4]. The samples were placed in a carburizing medium at a specific temperature for a certain period during the carburizing treatment (CT). The treated sample forms a specific carbon concentration gradient from the surface to the sub-surface [5]. The surface and sub-surface hardness of the sample were significantly improved after carburizing, while the core still maintained the same toughness as the original sample [6]. Xiao et al. [7] found that a high-hardness hardening layer and a residual compressive stress layer were produced on the vacuum-carburized sample's surface, effectively improving the surface properties of 20CrNiMo. Shengwei Qin et al. [8] found that when carburizing 18CrNiMo7-6 steel, by controlling the reasonable carburized layer depth, the surface properties of the sample can be improved.

The surface strain-strengthening treatment improves the performance of the surface layer of the component through plastic deformation. Plastic deformation at ultra-high

strain rates introduces residual compressive stress, grain refinement, and surface hardening [9]. Laser-shock peening (LSP) is a surface strain process that improves the surface properties of components effectively [10]. Li W. et al. [11] studied the effect of LSP on AISI 321 stainless steel. The results showed that LSP can significantly improve the surface hardness of the material, and the main reason is the dislocation density increasing. Zhou Liucheng et al. [12] found that the residual compressive stress in the surface layer of strengthened Ti-6Al-4V titanium alloy is significantly increased by LSP, and the crystalline grains are refined effectively. The research of Ho H. et al. [13] and Song Jingdong et al. [14] showed that residual compressive stress and grain refinement were beneficial to improving the bending fatigue and contact fatigue performance of metal components.

However, a single surface modification has improved the performance of the material, but the improvement is limited, and it cannot meet the needs of high-end equipment's key components. The hybrid modification of gear materials by phase change and strain is worthwhile for study.

In this study, 20CrNiMo samples were treated by CT, LSP, and CT + LSP, respectively. The samples' surface hardness, surface residual stress, microstructure, grain size, and surface toughness were compared in detail. The results were useful for improving the service performance of 20CrNiMo alloy steel components.

2. Materials and Methods

2.1. Experimental Materials

The material is 20CrNiMo steel, and its chemical composition (wt.%) is shown in Table 1. The size of the sample was 20 mm × 20 mm × 6 mm.

Table 1. Chemical composition of 20CrNiMo steel(wt.%).

Elemental Composition	C	Si	Mn	Cr	Ni	Mo	Fe
Content	0.21	0.29	0.75	0.55	0.5	0.2	BaL.

2.2. Sample Preparation

The original samples were quenched and tempered (QT). The purpose of QT was to make the material structure uniform, reduce the internal residual stress, improve the machining quality, and reduce the deformation during the subsequent carburizing treatment [15]. The QT samples were divided into four groups. The first group of samples was not subjected to subsequent treatment, with this treatment process represented as QT. After QT treatment, the second group of samples was subjected to LSP. This treatment process is represented as QT + LSP. The LSP principle is shown in Figure 1. With a short pulse and high peak power density, the laser beam passes through the constraint layer (generally the deionized water layer) and shines on the absorption layer. After absorbing laser energy, the absorbing layer material will produce high-pressure plasma. Due to the existence of the constraint layer, the plasma bombardment wave will impact the sample's surface, generating stress waves, which will cause plastic strain on the sample's surface. After the shock wave, the residual compressive stress field will be formed on the material's surface due to the self-balance effect of the internal force of the sample. The constraining layer was made of 2 mm thick flowing deionized water, and the absorption layer was made of 0.1 mm thick black tape. The laser-shock processing parameters mainly depend on the material [16]. By considering the properties of 20CrNiMo steel, the specific process parameters of LSP are shown in Table 2.

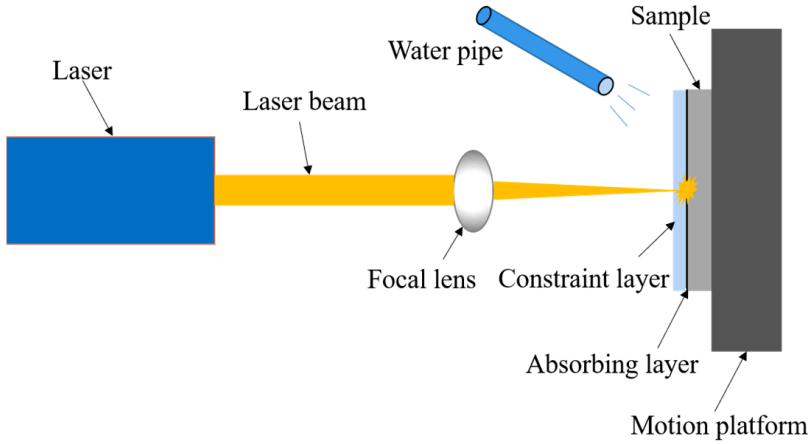


Figure 1. Schematic diagram of laser-shock processing.

Table 2. Process parameters of laser-shock processing.

Process	Laser Energy (J)	Pulse Width (ns)	Spot Diameter (mm)	Overlap Ratio
LSP	6	20	3	50%

The third group of samples was treated with CT after QT, and the treatment process is represented as QT + CT. The phase transition temperature of 20CrNiMo is about 850 °C, and the required carburizing depth is more than 1 mm. Therefore, the carburizing temperature was 920 °C, the carburizing time was 4 h, with a carbon potential of 1.2%, and the diffusion was 3 h, with a carbon potential of 0.9%. The mixed gas composed of 50% acetylene and 50% nitrogen was used as the carburizing atmosphere. Then, oil quenching was carried out at 860 °C, and finally, tempering was carried out at 160 °C for two hours. The specific carburizing heat treatment process is shown in Figure 2.

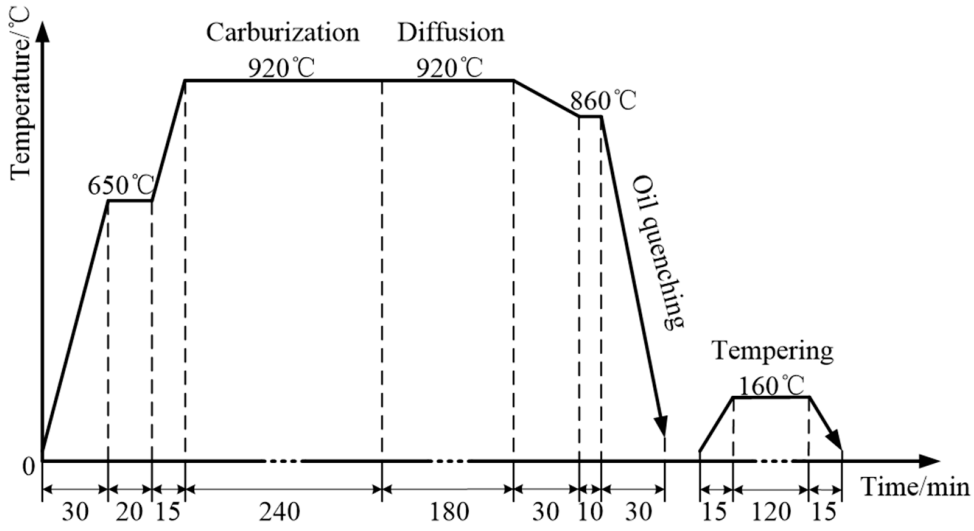


Figure 2. Process flow chart of carburizing heat treatment.

The fourth group of samples was treated with CT treatment and LSP surface modification treatment successively. QT + CT + LSP represents the composite treatment process. The carburizing process is shown in Figure 2, and the laser-shock processing parameters are shown in Table 2.

2.3. Testing and Characterization Methods

A FALCAN—511 digital Vickers microhardness tester (Vickers, London, UK) was utilized to measure the hardness and toughness of the surface layers of the four process samples. In the depth direction, hardness measurements were made at the first 9 points at intervals of 25 μm, the middle 8 points at intervals of 100 μm, and the last 6 points at intervals of 200 μm. An HDS-I X-ray residual stress tester (Aiste, Shanghai, China) and the roll fixation Ψ test were adopted to obtain the residual stress, calculated by the cross-correlation method. Electrolytic polishing was performed to remove surface materials layer by layer, and residual stress was measured at 50 μm each.

The sample cross-section was etched with a 4% nitric acid alcohol solution, and the surface microstructures of the four process samples were observed with a KEYENCE VK-X1000 confocal microscope (Keyence, Osaka, Japan). The characteristic diffracted crystal planes of the four process samples were studied using an X, Pert PRO X-ray diffractometer (XRD, Panalytical, Holland, The Netherlands), and the FWHM under different surface treatment processes was measured to characterize the grain changes under different treatment processes qualitatively. During the detection of FWHM, Cu-K was used for radiation, the working voltage was 40 Kv, the operating current was 40 mA, and the scanning angle range was 5~80°. Electron Back Scatter Diffraction (EBSD) analysis was carried out with the use of a Zeiss Sigma 500 scanning electron microscopy (SEM, Carl Zeiss AG, Oberkochen, Germany) system.

3. Results

3.1. Hardness

LSP and CT increase the hardness of materials based on phase-change strengthening and strain strengthening. To evaluate the hardening depth, in-depth micro-hardness measurements were performed on the cross-section of the QT sample, the QT + LSP sample, the QT + CT sample, and the QT + CT + LSP composite treatment sample, as shown in Figure 3.

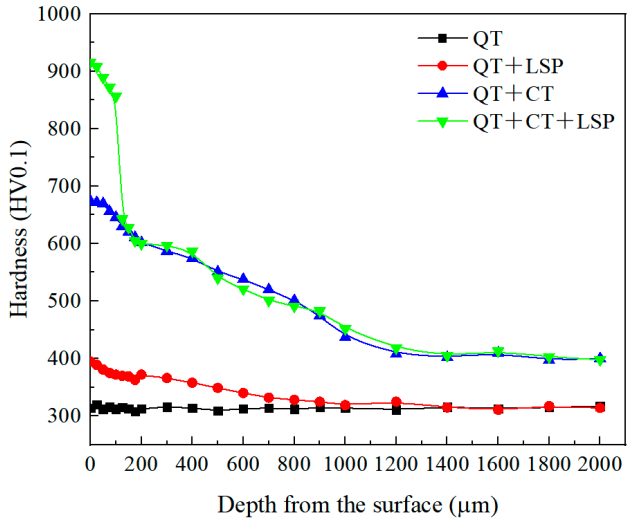


Figure 3. Microhardness in depth direction of different surface treatment processes.

It can be seen from Figure 3 that the microhardness of the QT sample is 314HV0.1. The surface hardness of the QT + LSP sample, QT + CT, and QT + CT + LSP composite treatment sample is higher than the core. The surface hardness of the sample decreases gradually along the depth direction and finally approaches the matrix hardness, showing a gradient distribution. The hardness-influencing layer of QT + LSP is about 1000 μm. Its surface hardness is 395HV0.1, which is 81HV0.1 higher than the matrix sample. The surface hardness of the QT + CT and QT + CT + LSP samples is 674HV0.1 and 916HV0.1, which are

360HV0.1 and 602HV0.1 higher than that of the base sample, respectively. In addition, the hardness-influencing layer of the QT + CT sample is 1800 μm. The hardness-influencing layer of the QT + CT + LSP composite treatment sample is 125 μm compared with the QT + CT sample.

During LSP, the material surfaces undergo ultra-high strain rate plastic deformation, resulting in strain hardening and improved micro-hardness. The QT + CT + LSP composite treatment sample showcases combined phase transformation and strain treatment characteristics, yielding the highest surface hardness. This high-hardness surface layer enhances the sample's fatigue resistance and hinders the initiation and propagation of cracks on the material surface [17].

CT treatment increases the hardness of 20CrNiMo's surface and core after QT, and the increase in the core is relatively less. LSP greatly increases the surface hardness on the basis of CT. When the surface hardness is increased, the overall bearing capacity is enhanced, the wear resistance can also be enhanced, and the core maintains the original toughness, which is conducive to the enhancement of impact resistance.

The improvement of the surface microhardness of 20CrNiMo makes its components have better wear resistance and impact resistance capacity.

3.2. Residual Stress

Different modification treatments can bring different residual compressive stress distributions to the surface layer of 20CrNiMo steel. The residual stress distribution in the depth direction is different for the QT sample, QT + LSP sample, QT + CT sample, and QT + CT + LSP sample. As shown in Figure 4, the QT sample has a residual stress layer with a small stress value, appearing in the near-surface layer of the sample with a depth of about 300 μm. The residual stress of the QT sample is introduced during the pre-processing of the sample, such as grinding and polishing, and it is stable at zero when the depth reaches about 300 μm. Compared with the QT sample, the surface residual stress value of the QT + LSP sample reaches −324 MPa. However, the maximum residual compressive stress appears on the sub-surface, 250 μm away from the surface, and the maximum value is −418 MPa. Meanwhile, with the increase in depth, the residual compressive stress increases first and then decreases. When the depth reaches about 1100 μm, the residual compressive stress disappears. The surface residual compressive stress of the QT + CT sample is −103 MPa, reaching a maximum value of −240 MPa at 150 μm from the surface. The residual compressive stress stabilizes at a zero-stress state after the depth exceeds 1050 μm from the surface. The surface residual compressive stress of QT + CT + LSP composite treatment reaches −635 MPa, which significantly increases compared with that of laser-shock or carburizing treatment. At the same time, the compressive residual stress decreases with an increase in depth. When the depth reaches 400 μm, the introduced residual compressive stress is consistent with the trend of the QT + CT sample. The depth of the residual stress-affected layer in the composite treatment is similar to LSP alone but has a greater impact on the value.

The high residual compressive stress on the specimen surface can inhibit fatigue crack initiation and delay crack growth [18]. Due to the structural transformation and grain refinement brought about by carburizing and laser-shock processing, the lattice distortion of the surface microstructure is induced, thus generating residual compressive stress [19,20]. The high residual compressive stress in the surface layer shifts the crack source region from the surface to the subsurface, and the cracks sprouting in the subsurface layer under the same rotational bending fatigue experimental conditions are subjected to less stress, which also inhibits them from expanding further into the interior of the material [21–23].

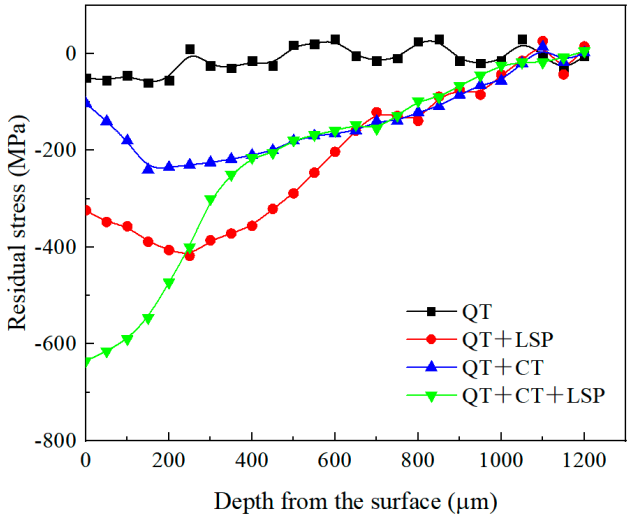


Figure 4. Residual stress in the depth direction of different surface treatment processes.

3.3. Microstructure

In addition to the changes in hardness and residual compressive stress, different modification treatments will also bring changes in surface microstructure. Figure 5 shows the surface microstructure of the QT sample, QT + LSP sample, QT + CT sample, and QT + CT + LSP composite treatment sample. As shown in Figure 5a, the metallographic structure of the QT sample, without laser-shock strengthening, primarily consists of tempered sorbite and pearlite. Figure 5b reveals that after laser-shock treatment, the structure in the laser-affected layer is refined, with the shocked pearlite exhibiting a finer texture compared to the unshocked counterpart. This suggests that the material's pearlite is refined by the action of the laser shock wave.

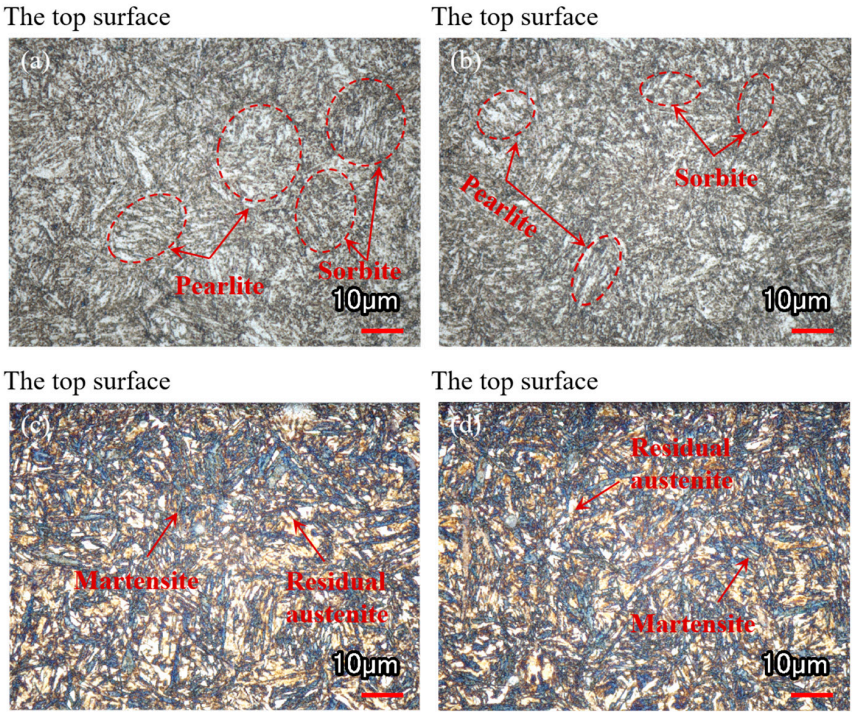


Figure 5. Surface microstructure of QT sample, QT + LSP sample, QT + CT sample, and QT + CT + LSP composite treatment sample; (**a**) QT sample, (**b**) QT + LSP sample, (**c**) QT + CT sample, (**d**) QT + CT + LSP composite treatment sample.

The structures depicted in Figure 5c,d consist of martensite and retained austenite. In Figure 5d, when combined with carburizing, the laser-shock treatment leads to a decrease in the austenite content in the surface layer due to the influence of stress.

Previous studies have shown that [24,25] the residual austenite is transformed into martensite under stress. Part of the retained austenite is transformed into hardened martensite, which significantly improves the surface hardness of the carburized layer. Residual austenite can release stress concentration under the action of force. A larger quantity of austenite will cause more obstacles to fatigue crack growth, thus improving fatigue life. This is attributed to the strain-induced phase transformation mechanism. The transformation of residual austenite to martensite was induced by laser-shock peening in advance, and the phase transformation at the crack tip was reduced during service so the stress at the crack tip was reduced. The transition from residual austenite to martensite slows down crack growth and reduces the crack growth rate. Secondly, the inherent toughness of austenite also plays a beneficial role in the generation and propagation of cracks.

3.4. XRD Analysis

In order to evaluate the change of crystallite size on the surface, XRD tests were carried out on samples with different modifications. The XRD patterns of the samples are shown in Figure 6. It was observed from Figure 6a that the results in different treatment states were similar, which showed that the composition of the prepared materials was consistent. From the magnified image in Figure 6b, it was found that the (110) diffraction peak gradually broadened from the QT state to the QT + CT + LSP state. The reduction in crystallite size on the material surface leads to the diffraction peak width increasing. Simultaneously, the position of the (110) diffraction peaks gradually moved to be left. The changes mentioned above indicate that, after different strengthening treatments, the surface material layers of samples appeared to have grain refinement and increased residual compressive stress in varying degrees. Among them, the crystallite size of the QT + CT + LSP sample was the smallest and its stress value was the highest. Grain refinement and residual compressive stress are beneficial in improving fatigue strength [26,27].

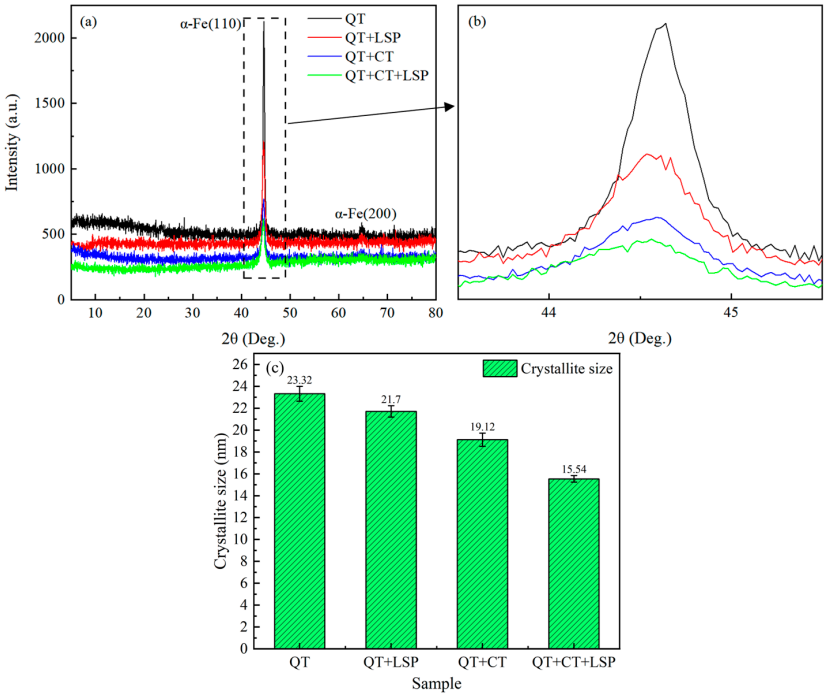


Figure 6. XRD spectrum of 20CrNiMo steel under different surface treatment processes. (**a**) XRD 2θ Angle pattern; (**b**) Magnification of the peak value spectrum at (**a**); (**c**) Crystallite size under different surface treatment processes.

The crystallite size of the specimen top surface can be calculated using the Debye–Scherrer [28] equation:

$$D = \frac{k\lambda}{\beta cos\theta}$$

where D is the average crystallite size, k is the shape factor of the lattice constant, λ is the wavelength of the X-ray radiation, and θ is the Bragg angle.

The crystallite size, calculated from the Full Width at Half Maximum (FWHM) of the (110) diffraction peak as shown in Figure 6c, is of particular interest. It is evident from the figure that the size of the top-surface crystallites in the QT sample decreased from 23.32 nm to 21.7 nm and 19.12 nm after LSP or carburizing treatment, respectively. The top-surface crystalline refinement in the QT + CT + LSP sample, which underwent carburizing and LSP hybrid modification, is more pronounced, reducing to 15.54 nm. This indicates that carburizing, LSP, and hybrid modification treatments effectively refined the crystallites on the top surface of the 20CrNiMo steel. Moreover, the top-surface crystallite refinement achieved through hybrid modification was significantly superior to single strengthening treatments.

3.5. EBSD Analysis

With the modifications, the surface grain is refined, and the subsurface grain is also changed for 20CrNiMo steel. To characterize the subsurface grain refinement, the microstructures below the surface of QT + CT and QT + CT + LSP samples were investigated by EBSD analysis. Figure 7 shows the EBSD diagram of the QT + CT and QT + CT + LSP samples. Inverse pole diagram (IPF), grain boundary misorientation, and crystallite size at a depth of 5 μm from the surface were investigated.

The crystal orientation is vividly shown in Figure 7a,b. The QT + CT + LSP sample shows a crystal orientation change due to plastic deformation caused by dislocation movements during LSP, promoting crystallographic misalignment [29]. Figure 7a,b show the IPF for selected areas of QT + CT and QT + CT + LSP, respectively (red: [001], blue: [111], green: [011]). It can be seen that the crystallite size of QT + CT (Figure 7a) is coarser, while that of QT + CT + LSP (Figure 7b) is significantly finer, with a crystallite size of 0.53 μm after LSP (Figure 7d) smaller than that of the QT + CT sample (Figure 7c) of 1.10 μm. Moreover, the crystallite size of QT + CT and QT + CT + LSP samples smaller than 1 μm accounted for 51% and 80%, respectively, as shown in Figure 7c,d. It can be seen that LSP makes the surface grain of the sample refined. During the LSP process, different dislocation motion is activated, such as tangle, recombination, annihilation, etc., causing grain refinement [19]. The surface grains of QT + CT + LSP samples were refined relative to those of QT + CT samples, resulting in an increase in large-angle grain boundaries on the surface of QT + CT + LSP samples, as shown in Figure 7e,f. Large-angle grain boundaries make crack propagation difficult, thus improving the toughness of the material [30].

3.6. Surface Toughness Test

The core hardness of the modified 20CrNiMo sample remained at the original level; while the surface hardness increased, the residual compressive stress was introduced, and the surface structure was refined. The core retains good toughness, and testing the surface toughness is helpful in understanding the matching degree between the surface properties of the modified 20CrNiMo sample and the core properties. This situation is similar to a metallic material with a surface coating, and the coating has a higher hardness and finer grain structure than the basis material. So the surface toughness of the modified 20CrNiMo steel was analyzed by observing the state of the material along the indentation edge in the indentation experiment, according to the 3198 guideline of VDI (Verein Deutscher Ingenieure) [31,32].

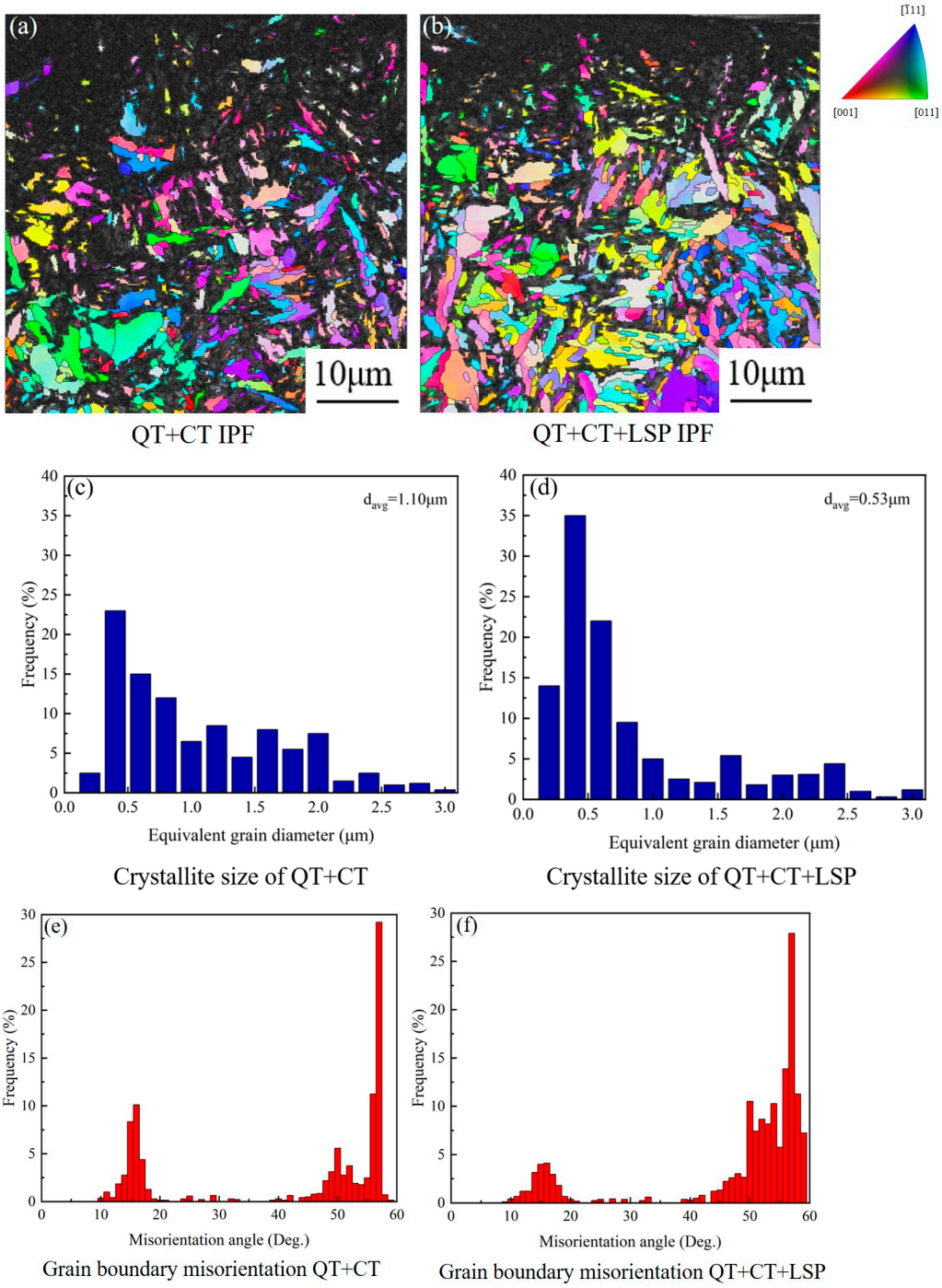


Figure 7. EBSD results of QT + CT and QT + CT + LSP; (**a**) QT + CT IPF, (**b**) QT + CT + LSP IPF. (**c**) Grain size of QT + CT. (**d**) Crystallite size of QT + CT + LSP. (**e**) Grain boundary misorientation of QT + CT. (**f**) Grain boundary misorientation of QT + CT + LSP.

To assess the impact of various surface treatment processes on sample surface toughness, an indentation test was conducted on the following samples: QT, QT + LSP, QT + CT, and QT + CT + LSP. The test involved applying a 9.8 N load for 10 s. It can be seen from Figure 8a,b that after the indentation test, there are many cracks near the indentation of the QT sample and QT + LSP sample. The number of cracks on the LSP sample is relatively less than the QT sample. This is due to the fact that the laser-shock strengthening improves the hardness of the surface layer of the sample, and the microstructure is refined at the same time. Therefore, the surface toughness of the surface layer of the sample is

improved to reduce the generation of microcracks. Figure 8c shows the QT + CT sample. It can be seen from the figure that there are a few cracks near the indentation of the CT sample, with notably fewer cracks compared to the QT sample. This is due to a large amount of high-carbon martensite generated on the surface of the CT sample, which caused the hardness to increase and the surface toughness to improve. Its surface toughness is higher than that of the QT and LSP samples. Figure 8d shows the surface appearance of the QT + CT + LSP sample after the indentation test. When carburizing and laser-shock composite treatment are performed, there is no crack on the sample's surface. The main reason is that laser-shock peening is performed based on carburizing, the microstructure in the surface layer is compact, and the grain in the surface layer of the sample is refined. At the same time, the hardness and strength are improved, and the surface toughness is further improved. At the same time, the residual compressive stress can offset part of the tensile stress on the surface area and improve its surface toughness. The surface toughness of the QT + CT + LSP sample is best.

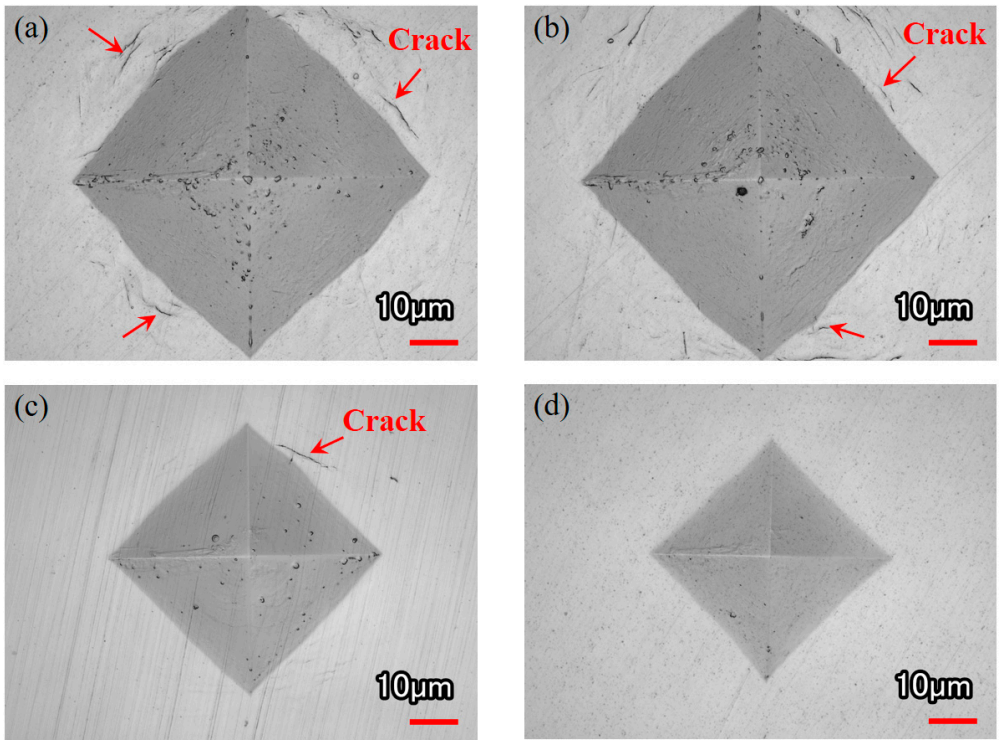


Figure 8. Surface toughness test results of QT sample, QT + LSP sample, QT + CT sample, and QT + CT + LSP composite treatment sample; (**a**) QT sample, (**b**) QT + LSP sample, (**c**) QT + CT sample, (**d**) QT + CT and LSP composite treatment sample.

3.7. Characterization of Mechanical Properties

The mechanical properties of the samples are shown in Figure 9. Compared with the QT sample, the yield strength of the QT + CT specimen increased from 768 MPa to 1280 MPa, and its tensile strength also increased from 985 MPa to 1623 MPa, which were increases of 66.7% and 64.8%, respectively. However, the yield strength and tensile strength of the QT + LSP specimens did not show any significant change, with the yield strength only increasing from 768 MPa to 803 MPa and the tensile strength only changing from 985 MPa to 1044 MPa. Comparing the yield and tensile strengths of the QT + CT sample with those of the QT + CT + LSP sample, we similarly found that there was no significant increase in yield and tensile strengths before and after LSP, which is in line with the findings of He Zhaoru et al. [33] and G. Muthukumaran et al. [34]. Therefore, we think that the influence of carburizing treatment on the mechanical properties of 20CrNiMo steel plays a leading role, while LSP has less influence on the overall mechanical properties of the specimen.

This is because LSP primarily improves the surface properties of the specimen, whereas the yield strength and tensile strength of the specimen pertain to macro-level properties.

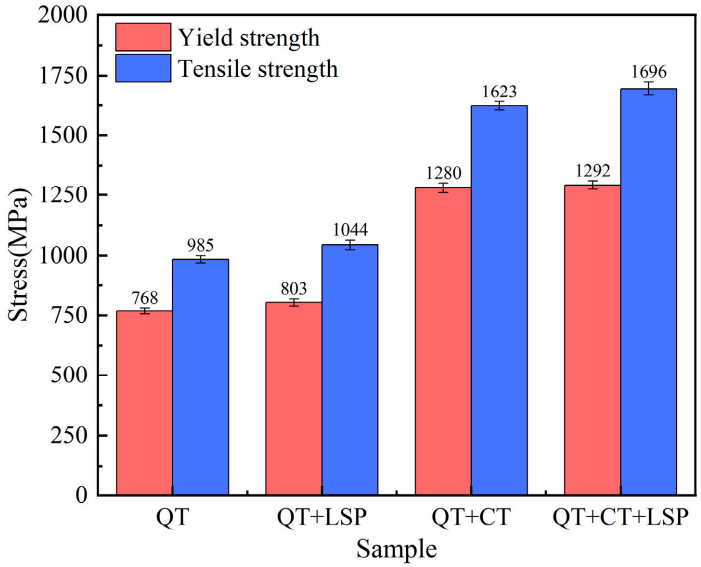


Figure 9. Yield strength and tensile strength of QT sample, QT + CT sample, QT + LSP sample, and QT + CT + LSP sample.

4. Discussion

The results above show that the surface hardness, surface residual compressive stress, grain refinement, and toughness of the sample after QT + CT + LSP composite treatment were significantly higher than individual laser-shock peening and carburizing treatment. Figure 9 shows the schematic diagram of the composite treatment of carburizing and laser shocking. As shown in Figure 10a,b, the QT samples were carburized, the heart tissue changed from pearlite and sorbite to lath martensite, and the heart maintained good toughness. The surface layer was transformed into acicular martensite. The acicular martensite has high hardness, which effectively improved the sample's mechanical properties and enabled the carburized sample to have a high bearing capacity [19]. Laser-shock peening was carried out based on carburizing treatment, and a strain-strengthening layer was formed on the surface of the sample, as shown in Figure 10c. After composite treatment, the sample material was transformed into a composite strengthening layer with the carburized surface, laser shocking, carburized strengthening layer in the middle, and a gradient structure material with a lath martensite layer in the core. The strengthening layer was divided into two parts: the composite strengthening layer of CT and LSP on the surface layer, which is about 100 μm thick; and the carburizing layer, which is about 1.8 mm thick. As for the composite strengthening layer, the surface strength and hardness of the sample were improved, the residual stress of the surface layer was prefabricated, and the surface microstructure was refined. The refinement of surface microstructure resulted in grain refinement. The 20CrNiMo gear, with this functional gradient structure, could withstand greater impact stress due to its lath martensite core and good toughness. The composite strengthening layer and carburized layer had higher hardness and strength. And the composite strengthening layer had more considerable residual compressive stress, which could withstand more significant cyclic stress and impact force. This means that a gear made of 20CrNiMo material could obtain better service performance after composite treatment.

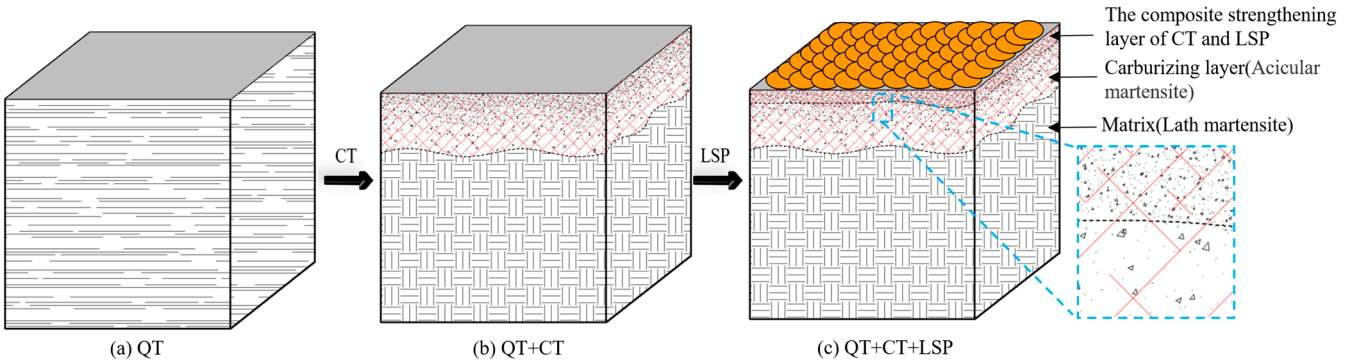


Figure 10. (**a**–**c**) Schematic diagram of material structure after carburizing and laser-shocking treatment.

5. Conclusions

To meet the stress requirements of gears in service, the carburizing, the laser shocking, the composite treatment of laser shocking and carburizing were carried out on 20CrNiMo steel, and the changes in hardness, residual stress, microstructure, and toughness were obtained under different process methods. Through the analogical method, this study found:

1. After carburizing, the hardness of the 20CrNiMo sample significantly increased, and the maximum surface hardness increased by 674HV0.1. The microhardness of the sample with carburizing and laser-shock hybrid modification treatment increased to 916HV0.1.

2. Laser-shock processing brought high compressive residual stress to the 20CrNiMo sample; especially on the basis of the carburized sample, the residual compressive stress was increased to about 635 MPa.

3. Based on the carburized sample, laser shocking refined the surface grain to 0.53 μm and made the toughness best.

4. After the composite treatment of carburizing and laser shocking, a functionally graded material was obtained for the 20CrNiMo sample. The functionally graded material had a laser shocking + carburizing composite peening layer, a carburizing layer, and a matrix. The surface layer of the functionally graded structural materials had the characteristics of super-hardness, high compressive residual stress, good toughness, and grain refinement.

Some of the laws obtained in the paper are similar to those of the carburizing treatment of 18CrNiMo7-6 steel and the enhancement of the surface properties of 30CrMnSiNi2A steel after laser-shock peening [6,35], which indicates that the application of carburizing and laser impact modification in improving the performance of 20CrNiMo gear steel has significant effects and the method is reasonable. The effect of carburizing and laser-shock peening hybrid modification on the service performance of 20CrNiMo gear steel can be further investigated.

Author Contributions: Conceptualization, X.C. and Z.X.; methodology, X.C. and J.S.; validation, X.C., J.C. and B.G.; formal analysis, K.L.; investigation, Y.L.; resources, X.C., Z.X. and Q.J.; data curation, J.C.; writing—original draft preparation, X.C. and J.S.; writing—review and editing, X.C. and B.G.; visualization, Q.J. and J.C.; supervision, J.C.; project administration, Z.X.; funding acquisition, X.C., J.C. and Q.J.; All authors have read and agreed to the published version of the manuscript.

Funding: This research was funded by Natural Science Foundation of Fujian, China (Grant No.2021J05168), The Major Science And Technology Projects of Fujian, China (Grant No.2021HZ024006, 2022HZ024009), The Marine Economic Development Project of Fujian, China (Grant No. FJHJF-L-2021-9) and Major Science and Technology Project in Xiamen City (Grant No. 3502Z20231011, 3502Z20231001).

Data Availability Statement: The data presented in this study are available on request from the corresponding author.

Conflicts of Interest: The authors declare no conflict of interest.

References

1. Luo, S.; Shen, Z.; Yu, Z.; Wang, W.; Zhu, M. Effect of Ce Addition on Inclusions and Grain Structure in Gear Steel 20CrNiMo. *Steel Res. Int.* **2020**, *92*, 2000394. [CrossRef]
2. Feng, W.; Feng, Z.; Mao, L. Failure analysis of a secondary driving helical gear in transmission of electric vehicle. *Eng. Fail. Anal.* **2020**, *117*, 104934. [CrossRef]
3. Dong, M.; Cui, X.; Zhang, Y.; Jin, G.; Yue, C.; Zhao, X.; Cai, Z.; Xu, B. Vacuum carburization of 12Cr2Ni4A low carbon alloy steel with lanthanum and cerium ion implantation. *J. Rare Earths* **2017**, *35*, 1164–1170. [CrossRef]
4. Wang, J.; Qu, S.; Shao, H.; Hu, X.; Guo, B.; Li, X. Ultra-high fatigue property and fracture mechanism of modified 20CrMoH steel by gas carburizing technology combined with shot peening treatment. *Int. J. Fatigue* **2022**, *165*, 107221. [CrossRef]
5. Chu, Y. The Evolution of Microstructure for Carburizing and Quenching 17CrNiMo6 Steel Forecasting and Experimentation. *Coatings* **2022**, *12*, 1102. [CrossRef]
6. Xu, G.; Luo, J.; Lu, F.; Wang, G.; Liu, H.; Zhao, M. Characterization of fracture toughness for surface-modified layer of 18CrNiMo7-6 alloy steel after carburizing heat treatment by indentation method. *Eng. Fract. Mech.* **2022**, *269*, 108508. [CrossRef]
7. Xiao, N.; Hui, W.; Zhang, Y.; Zhao, X.; Chen, Y.; Dong, H. High cycle fatigue behavior of a low carbon alloy steel: The influence of vacuum carburizing treatment. *Eng. Fail. Anal.* **2020**, *109*, 104215. [CrossRef]
8. Qin, S.; Zhang, C.; Zhang, B.; Ma, H.; Zhao, M. Effect of carburizing process on high cycle fatigue behavior of 18CrNiMo7-6 steel. *J. Mater. Res. Technol.* **2022**, *16*, 1136–1149. [CrossRef]
9. Gu, H.; Yan, P.; Jiao, L.; Chen, S.; Song, Y.; Zou, S.; Wang, X. Effect of laser shock peening on boring hole surface integrity and conformal contact fretting fatigue life of Ti-6Al-4 V alloy. *Int. J. Fatigue* **2023**, *166*, 107241. [CrossRef]
10. Pan, X.; Gu, Z.; Qiu, H.; Feng, A.; Li, J. Study of the Mechanical Properties and Microstructural Response with Laser Shock Peening on 40CrMo Steel. *Metals* **2022**, *12*, 1034. [CrossRef]
11. Li, W.; Chen, H.; Huang, W.; Chen, J.; Zuo, L.; Li, C.; He, J.; Ren, Y.; Zhang, S. Effect of laser shock peening on high cycle fatigue properties of aluminized AISI 321 stainless steel. *Int. J. Fatigue* **2021**, *147*, 106180. [CrossRef]
12. Zhou, L.; Pan, X.; Shi, X.; Du, T.; Wang, L.; Luo, S.; He, W.; Chen, P. Research on surface integrity of Ti-6Al-4V alloy with compound treatment of laser shock peening and shot peening. *Vacuum* **2022**, *196*, 110717. [CrossRef]
13. Ho, H.S.; Li, D.L.; Zhang, E.L.; Niu, P.H. Shot Peening Effects on Subsurface Layer Properties and Fatigue Performance of Case-Hardened 18CrNiMo7-6 Steel. *Adv. Mater. Sci. Eng.* **2018**, *2018*, 3795798. [CrossRef]
14. Song, J.; Luo, S.; Liang, X.; Cao, Z.; Zhao, W.; Pu, C.; He, W. Rolling contact fatigue and damage characteristic of AISI 9310 steel with pre-laser shock peening treatment. *Int. J. Fatigue* **2022**, *155*, 106588. [CrossRef]
15. Dannoshita, H.; Hasegawa, H.; Higuchi, S.; Matsuda, H.; Gong, W.; Kawasaki, T.; Harjo, S.; Umezawa, O. Evolution of dislocation structure determined by neutron diffraction line profile analysis during tensile deformation in quenched and tempered martensitic steels. *Mater. Sci. Eng. A* **2022**, *854*, 143795. [CrossRef]
16. Chen, X.; Sun, J.; Xu, Z.; Chen, J.; Jiang, Q.; Li, Y.; Li, J.; Cheng, J. Optimization of Laser Shock Process Parameters for 40Cr Steel. *Coatings* **2022**, *12*, 1872. [CrossRef]
17. Luo, S.; He, W.; Chen, K.; Nie, X.; Zhou, L.; Li, Y. Regain the fatigue strength of laser additive manufactured Ti alloy via laser shock peening. *J. Alloys Compd.* **2018**, *750*, 626–635. [CrossRef]
18. Luo, X.; Dang, N.; Wang, X. The effect of laser shock peening, shot peening and their combination on the microstructure and fatigue properties of Ti-6Al-4V titanium alloy. *Int. J. Fatigue* **2021**, *153*, 106465. [CrossRef]
19. Cao, J.; Cao, X.; Jiang, B.; Yuan, F.; Yao, D.; Huang, J. Microstructural evolution in the cross section of Ni-based superalloy induced by high power laser shock processing. *Opt. Laser Technol.* **2021**, *141*, 107127. [CrossRef]
20. Minamizawa, K.; Arakawa, J.; Akebono, H.; Nambu, K.; Nakamura, Y.; Hayakawa, M.; Kikuchi, S. Fatigue limit estimation for carburized steels with surface compressive residual stress considering residual stress relaxation. *Int. J. Fatigue* **2022**, *160*, 106846. [CrossRef]
21. Sun, Y.; Liu, W.J.; Zhang, H.W. Simulation of Residual Stress Evolution of 8Cr4Mo4V Steel Induced by Laser Shock and Its Influence on Fatigue Performance. *Chin. J. Mater. Res.* **2023**, 1–12. Available online: http://kns.cnki.net/kcms/detail/21.1328.TG.20231017.1623.002.html (accessed on 2 December 2023).
22. Lu, W.; Zhang, C.; Luan, S. Quantifying effect of overload-induced residual stress behind crack tip on fatigue crack growth. *Eng. Fract. Mech.* **2023**, *292*, 109593. [CrossRef]
23. Jiang, Q.; Zhu, L.; Chen, J.; Chen, X.; Weng, J.; Xu, Z.; Zhao, Z. The Effects of Ultrasonic Impact Modification on the Surface Quality of 20CrNiMo Carburized Steel. *Coatings* **2023**, *13*, 1594. [CrossRef]
24. Kanetani, K.; Mikami, T.; Ushioda, K. Effect of Retained Austenite on Sub-surface Initiated Spalling during Rolling Contact Fatigue in Carburized SAE4320 Steel. *ISIJ Int.* **2020**, *60*, 1774–1783. [CrossRef]
25. Roy, S.; Sundararajan, S. The effect of heat treatment routes on the retained austenite and Tribomechanical properties of carburized AISI 8620 steel. *Surf. Coat. Technol.* **2016**, *308*, 236–243. [CrossRef]
26. Yang, K.; Huang, Q.; Zhong, B.; Wang, Q.; Chen, Q.; Chen, Y.; Su, N.; Liu, H. Enhanced extra-long life fatigue resistance of a bimodal titanium alloy by laser shock peening. *Int. J. Fatigue* **2020**, *141*, 105868. [CrossRef]
27. Yang, F.; Liu, P.; Zhou, L.; He, W.; Pan, X.; An, Z. Review on Anti-Fatigue Performance of Gradient Microstructures in Metallic Components by Laser Shock Peening. *Metals* **2023**, *13*, 979. [CrossRef]
28. Warren, B.E. *X-ray Diffraction*; Courier Corporation: Chelmsford, MA, USA, 1990.

29. Dhakal, B.; Swaroop, S. Effect of laser shock peening on mechanical and microstructural aspects of 6061-T6 aluminum alloy. *J. Mater. Process. Technol.* **2020**, *282*, 116640. [CrossRef]
30. Karthik, D.; Yazar, K.U.; Bisht, A.; Swaroop, S.; Srivastava, C.; Suwas, S. Gradient plastic strain accommodation and nanotwinning in multi-pass laser shock peened 321 steel. *Appl. Surf. Sci.* **2019**, *487*, 426–432. [CrossRef]
31. Zamharir, M.J.; Aghajani, H.; Tabrizi, A.T. Evaluation of adhesion strength of TiN layer applied on 316L substrate by electrophoretic deposition. *J. Aust. Ceram. Soc.* **2021**, *57*, 1219–1230. [CrossRef]
32. Li, N.; Hong, Y.; Wu, C.L.; Xu, Q. Gaseous Nitrocarburizing and Post-quenching of Low Carbon Steel. *Surf. Technol.* **2018**, *47*, 5–16. [CrossRef]
33. He, Z.; Shen, Y.; Tao, J.; Chen, H.; Zeng, X.; Huang, X.; El-Aty, A.A. Laser shock peening regulating aluminum alloy surface residual stresses for enhancing the mechanical properties: Roles of shock number and energy. *Surf. Coat. Technol.* **2021**, *421*, 127481. [CrossRef]
34. Muthukumaran, G.; Rai, A.K.; Gautam, J.; Babu, P.D.; Ranganathan, K.; Bindra, K.S. A Study on Effect of Multiple Laser Shock Peening on Microstructure, Residual Stress, and Mechanical Strength of 2.5 Ni-Cr-Mo (EN25) Low-Alloy Steel. *J. Mater. Eng. Perform.* **2022**, *32*, 4361–4375. [CrossRef]
35. Shu, S.; Shen, Y.; Cheng, Z.; Xiong, W.; He, Z.; Song, S.; Liu, W. Laser shock peening regulating residual stress for fatigue life extension of 30CrMnSiNi2A high-strength steel. *Opt. Laser Technol.* **2024**, *169*, 110094. [CrossRef]

Disclaimer/Publisher's Note: The statements, opinions and data contained in all publications are solely those of the individual author(s) and contributor(s) and not of MDPI and/or the editor(s). MDPI and/or the editor(s) disclaim responsibility for any injury to people or property resulting from any ideas, methods, instructions or products referred to in the content.